Multistep IgE Mast Cell Desensitization Is a Dose- and Time-Dependent Process Partially Regulated by SHIP-1

Ather Adnan,[*,†] Shree Acharya,[*] Leila A. Alenazy,[*,‡] Leticia de las Vecillas,[*,§] Pedro Giavina Bianchi,[¶] Matthieu Picard,[‖] Lucia Calbache-Gil,[#,] Salvador Romero-Pinedo,[#,**] Ana Clara Abadía-Molina,[#,**] William Kerr,[††] Chiara Pedicone,[††] Jun Nagai,[*] Eleanor Hollers,[*] Daniel Dwyer,[*] and Mariana Castells[*]**

Multistep mast cell desensitization blocks the release of mediators following IgE crosslinking with increasing doses of Ag. Although its in vivo application has led to the safe reintroduction of drugs and foods in IgE-sensitized patients at risk for anaphylaxis, the mechanisms of the inhibitory process have remained elusive. We sought to investigate the kinetics, membrane, and cytoskeletal changes and to identify molecular targets. IgE-sensitized wild-type murine (WT) and FcεRIα humanized (h) bone marrow mast cells were activated and desensitized with DNP, nitrophenyl, dust mites, and peanut Ags. The movements of membrane receptors, FcεRI/IgE/Ag, actin, and tubulin and the phosphorylation of Syk, Lyn, P38-MAPK, and SHIP-1 were assessed. Silencing SHIP-1 protein was used to dissect the SHIP-1 role. Multistep IgE desensitization of WT and transgenic human bone marrow mast cells blocked the release of β-hexosaminidase in an Ag-specific fashion and prevented actin and tubulin movements. Desensitization was regulated by the initial Ag dose, number of doses, and time between doses. FcεRI, IgE, Ags, and surface receptors were not internalized during desensitization. Phosphorylation of Syk, Lyn, p38 MAPK, and SHIP-1 increased in a dose–response manner during activation; in contrast, only SHIP-1 phosphorylation increased in early desensitization. SHIP-1 phosphatase function had no impact on desensitization, but silencing SHIP-1 increased β-hexoxaminidase release, preventing desensitization. Multistep IgE mast cell desensitization is a dose- and time-regulated process that blocks β-hexosaminidase, impacting membrane and cytoskeletal movements. Signal transduction is uncoupled, favoring early phosphorylation of SHIP-1. Silencing SHIP-1 impairs desensitization without implicating its phosphatase function. ***The Journal of Immunology*****, 2023, 210: 709–720.**

Multistep IgE desensitization is achieved by dividing an activating Ag dose into multiple suboptimal doses and delivering the suboptimal doses sequentially at fixed time intervals, which blocks cell activation and inhibits the release of mediators, making mast cells refractory to optimal Ag (1–3). Mimicking this in vitro inhibitory process, human desensitization protocols have protected patients allergic to antibiotics, chemotherapy, mAbs, and other drugs and foods when reintroduced to their IgE-sensitizing allergens, preventing anaphylaxis and increasing their life expectancy and quality of life (4–9). Despite the proven safety and efficacy in thousands of highly allergic patients, breakthrough reactions and anaphylaxis are unpredictable, occurring in 25% of desensitization protocols, making the procedures high risk and hampering universal application (10). The perception that desensitization protocols remain empiric has spurred an impetus for a better understanding of the underlying inhibitory mechanisms and the pursuit of molecular targets.

IgE mast cell activation is a complex and well-studied process initiated by crosslinking of IgE-sensitized FcεRI receptors by multimeric Ags, which induces intracellular signaling and the acute and delayed release of inflammatory mediators (11, 12).

*Division of Allergy and Immunology, Department of Medicine, Brigham and Women's Hospital, Harvard Medical School, Boston, MA; [†]Texas A&M Health Science Center, College of Medicine, Houston, TX; [‡]Division of Allergy and Clinical Immunology, Department of Medicine, College of Medicine, King Saud University, Riyadh, Saudi Arabia; [§]Department of Allergy, Marqués de Valdecilla University Hospital – Instituto de Investigación Marques de Valdecilla, Santander, Spain; [¶]Clinical Immunology and Allergy Division, School of Medicine, Universidade de São Paulo, R. Prof. Artur Ramos Sao Paulo, Brazil; [‖]Division of Allergy and Clinical Immunology, Department of Medicine, Hôpital Maisonneuve-Rosemont, Université de Montréal, Montreal, QC, Canada; [#]Unidad de Inmunología, IBIMER, CIBM, Universidad de Granada, Granada, Spain; **Departamento de Bioquímica y Biología Molecular III e Inmunología, Facultad de Medicina, Universidad de Granada, Granada, Spain; and [††]Department of Microbiology and Immunology, SUNY Upstate Medical University, Syracuse, NY

ORCIDs: 0000-0001-9640-9916 (A.A.); 0000-0003-4969-5678 (L.d.l.V.); 0000-0003-3108-5804 (M.P.); 0000-0002-3147-3535 (A.C.A.-M.); 0000-0002-4720-7135 (W.K.); 0000-0002-9486-1746 (C.P.); 0000-0003-4720-5065 (J.N.); 0000-0002-5958-3090 (E.H.); 0000-0001-6451-0163 (M.C.).

Received for publication May 25, 2021. Accepted for publication December 22, 2022.

This work was supported by a postresidency contract "Wenceslao Lopez-Albo" provided by the Instituto de Investigacion Marques de Valdecilla-IDIVAL (Santander, Spain) (L.d.l.V.). L.C.-G. and S.R.-P. are Ph.D. students in the Official Doctoral Program in Biomedicine of the University of Granada. The research performed by L.C.-G., S.R.-P., and A.C.A.-M. was supported and funded by the Plan Estatal de Investigación Científica y Técnica y de Innovación 2013–2016, ISCIII-Subdirección General de Evaluación y Fomento de la Investigación, Ministerio de Economía y Competitividad, Spain (Grants PI16/01642 and PI10/01096), Plan Propio de la Universidad de Granada, Spain 2014 (Grant PP2014.01).

Address correspondence and reprint requests to Dr. Mariana Castells, Brigham and Women's Hospital, 60 Fenwood Road, Room 5002N, Boston, MA 02115. E-mail address: mcastells@bwh.harvard.edu

The online version of this article contains supplemental material.

Abbreviations used in this article: 3AC, 3α-aminocholestane; Der p or Dp, *Dermatophagoides pteronyssinus*; hBMMC, FcεRI chain humanized bone marrow–derived mast cell; HSA, human serum albumin; ITAM, immunoreceptor tyrosine-based activation motif; LAMP-1, lysosomal-associated membrane protein 1; mBMMC, murine bone marrow–derived mast cell; NP, nitrophenyl; SHIP1, SH2-containing inositol phosphatase 1; Tg, transgenic; WT, wild type.

Phosphorylation of the β- and γ-chain immunoreceptor tyrosine-based activation motifs (ITAMs) provides docking for upstream molecular players, leading to downstream signal transmission by second messengers, mobilization of intracellular calcium with extracellular calcium influx, and cytoskeletal movements led by actin and tubulin, whereas FcεRI–IgE–Ag complexes are internalized (13, 14). We and others have shown that this well-orchestrated machinery is halted by desensitization. Bone marrow–derived mast cells (BMMCs) sensitized with DNP-IgE and desensitized to an optimal dose of DNP administered as 11 sequential suboptimal doses cannot mobilize calcium, do not release granule mediators, do not generate PGs and leukotrienes from membrane arachidonic acid, and do not produce cytokines (3, 15). Although models of basophil IgE desensitization have provided some insight (16), how mast cells engage in this inhibitory pathway is poorly understood.

The fundamental questions of what amount of Ag can start the desensitization process, how to increase the doses without inducing signal transduction, and the time requirements have not been defined. Intriguingly, signal transduction is impaired during the final steps of desensitization when optimal Ag is reached, indicating that the initial steps have diverted activation partners. Although Syk phosphorylation is required to initiate signal transduction, recent data suggest that phosphatases such as SH2-containing inositol phosphatase 1 (SHIP-1) associate with the FcεRI–IgE–Ag complex and compete with Syk when Ag doses are delivered in quick sequence in contrast to more prolonged times (17–19). Quick Ag delivery leads to SHIP-1 activation and inhibitory signaling, indicating that the time between doses can dictate outcomes. This is consistent with the notion that the propagation of signal requires kinetic proofreading with enough receptor/ligand dwell time to generate activated receptor complexes that can progress to distal responses.

Rapidly dissociating ligands are less effective at generating distal responses. Whether SHIP interferes with signal propagation by reducing activation time is not known. The generation of signaling membrane domains with activation partners has been demonstrated, but the membrane arrangements during desensitization have not been defined (21), and the potential participation of immunoreceptor tyrosine-based inhibition motifs bearing inhibitory receptors such as gp49B1, which associate with phosphatases SHP-1, SHP-2, and SHIP-1 and dephosphorylate FcεRI ITAMs, is not known (22, 23). Although internalization of FcεRI–IgE–Ag complexes is not required for signal transduction at low Ag (13), it remains controversial whether internalization can initiate desensitization and if tubulin and actin can provide cytoskeletal support to the inhibitory state (1, 2). Here, we reproduce an in vitro model of IgE activation and desensitization (3, 15) using wild-type murine (WT mBMMCs) and FcεRIα-chain humanized mast cells (transgenic [Tg] hBMMCs) and provide the initial effective dose, dose progression, and time intervals for optimal Ag-specific desensitization, including inhalant and food allergens. We follow surface membrane and intracytoplasmic changes, including actin and tubulin movements and phosphorylation of Syk, Lyn, p38-MAPK, and SHIP-1, to assess the uncoupling of signal transduction. We show enhanced SHIP-1 phosphorylation during the early steps of desensitization, not associated with its phosphatase function. By silencing SHIP-1, desensitization is impaired, uncovering the first molecular target of multistep IgE desensitization.

Materials and Methods

Mice

Male WT BALB/c 8–12-wk-old mice were purchased from The Jackson Laboratory (Bar Harbor, ME). Tg BALB/c mice expressing the human FcεRIα (gift from Jean-Pierre Kinet, Beth Israel Deaconess Medical Center, Boston, MA) (24, 25) were bred at the Dana-Farber Cancer Institute Animal Resource Facility. Briefly, male mFcεRIα$^{-/-}$ mice carrying the transgene encoding hFcεRI were bred to females as described previously (26). Mice were euthanized by CO_2 asphyxiation.

Mast cell cultures

Tg BMMCs carrying the α-chain of the high-affinity IgE receptor FcεRI (Tg hBMMCα) and murine BMMCs (mBMMCs) were harvested from 8–12-wk-old WT murine femurs and cultured for 4–16 wk in RPMI 1640 medium supplemented with 10% FBS, 2 mM L-glutamine, 1% penicillin-streptomycin, 0.1 mM MEM nonessential amino acids (all from Sigma-Aldrich), and 10 ng/ml of IL-3 (3). IL-3 was obtained from supernatants of 293T cells expressing murine IL-3 (27) and from commercial sources (R&D Systems and PeproTech). All animal work was approved by the Dana-Farber Cancer Institute Animal Care and Use Committee (IACUC 2016N000552). WT mBMMCs (4×10^6 cells/ml) were sensitized with anti-DNP IgE (clone SPE-7; Sigma-Aldrich) at 1 μg/ml (0.25 μg/10^6 cells/ml) overnight at 37°C. Tg hBMMCs were incubated overnight with anti-nitrophenyl (anti-NP) IgE (0.5 mg/10^6 cells/ml, clone JW8/1; Bio-Rad Laboratories) at 37°C or with concentrated human serum diluted at 20% in RPMI (4×10^6 cells/ml) for 18–24 h at 37°C. Cells were then washed twice and resuspended at 1×10^6 cells/50 μl RPMI without IL-3 and distributed into tubes at 37°C for activation or desensitization. WT mBMMCs (50 μl/tube containing either 0.5×10^6 or 1×10^6 mBMMCs) were challenged with 50 μl of DNP-human serum albumin (DNP-HSA) and Tg hBMMCs with NP-BSA (Sigma-Aldrich) at 20 pg/μl or 200 pg/μl (1 ng, 10 ng) and, for control, with 50 μl of HSA or BSA at 20 pg/μl or 200 pg/μl (1 ng, 10 ng) or with dust mites and peanut allergens and, after 10 min in 37°C, placed on ice.

LAD2 cells

LAD2 cells were obtained from the National Institutes of Health (28) and cultured at 1×10^6 in StemPro34 serum-free medium with the StemPro media supplement (catalog no. 10639011; Life Technologies), L-glutamine (catalog no. G7513; Sigma-Aldrich), penicillin-streptomycin, and recombinant human stem cell factor (100 ng/ml, catalog no. 300-07; PeproTech). Cells were sensitized with human myeloma plasma IgE (Athens Research and Technology) at 5 μg/ml overnight at 37°C with 5% CO_2. Cells were then washed once with sterile HBSS and resuspended in warmed StemPro34 media (Life Technologies) (supplemented with StemPro nutrient supplement; Life Technologies), 2 mM L-glutamine (Sigma-Aldrich), 100 ng/ml recombinant human stem cell factor (PeproTech), 1% penicillin-streptomycin) at a concentration of 0.5×10^6 cells/ml and used in activation and desensitization experiments at 1×10^6 cells/ml.

Human serum

Informed consent was obtained from human subjects (institutional review board approval no. 2020P002043). Sera from one dust mite allergic individual (donor 1) and one peanut and dust mite allergic individual (donor 2) were concentrated by centrifugation at $4000 \times g$ for 1 h in 100 kDa centrifugal filter units (Merck Millipore) and stored at −20°C and used for sensitization of Tg hBMMCα. Donors 1 and 2 had positive skin test results, and serum allergen-specific IgE titers were determined by ImmunoCAP (Phadia). After concentration, donor 1 total IgE was 1127 ng/ml, and donor 2 total IgE was 545 ng/ml. Before concentration, donor 1 had *Dermatophagoides pteronyssinus* (Der p or Dp)-specific IgE of 40 kUA/L, and donor 2 had a Der p-specific IgE of 1.64 kUA/L and a peanut- specific IgE of 18.4 kU/L.

Mast cell activation

Dermatophagoides pteronyssinus *and peanut.* Tg hBMMCs were stimulated with Der p extract 30,000 AU/ml (Hollister-Stier, Spokane, WA) and/or peanut extract (1 μg/ml) (Greer, Lenoir, NC) in RPMI. Tg hBMMCs were activated as described for WT mBMMCs (Fig. 1A, Supplemental Fig. 1, and Supplemental Tables I–IV).

DNP and NP. WT mBMMCs (50 μl/tube containing either 1×10^6 or 0.5×10^6 BMMCs) were challenged with 50 μl of DNP-HSA and Tg hBMMCs with 4-hydroxy-3-NP-BSA (Sigma-Aldrich) at 20 pg/μl or 200 pg/μl (1 ng, 10 ng, respectively). A negative control, 50 μl of culture medium + 50 μl of HSA or BSA at 20 pg/μl or 200 pg/μl (1 ng, 10 ng, respectively), was used. After incubation for 10 min at 37°C, cells were placed on ice. For dose–response experiments, Ags were diluted in RPMI 1640 culture medium. Dose–response experiments were performed by adding 50 μl of varying Ag dilutions to 50 μl of cell suspension for 10 min at 37°C before the suspension was placed on ice.

Mast cell desensitization

Dermatophagoides pteronyssinus *and peanut.* Tg hBMMCα were desensitized to Der p and peanut Ags in incremental steps using the protocols described in Fig. 1A, Supplemental Fig. 1, and Supplemental Tables I–IV and based on a previously established protocol (15). For desensitization experiments with Der p and peanut Ags (Fig. 2B, 2C), the 11-step protocol in Supplemental Fig. 1A was used. Fig. 2A, 2B, and 2C used serum from donor 2, whereas experiments for Fig. 2D, 2E, and 2F used serum from donor 1. The target dose for activation in Fig. 2D, 2E, and 2F was 2.5 AU/ml. The protocols for experiments in Fig. 2D and 2E involved varying the number of total steps to achieve desensitization (Supplemental Fig. 1, Supplemental Tables I and II). The starting concentration of 0.02 AU/ml (Fig. 2D, 2F) was based on a dose–response curve showing that 0.02 AU/ml did not elicit significant activation (Fig. 2A) and was similar to 0.01 AU/ml (Fig. 2E). The protocol for Fig. 2D–2F is the eight-step protocol (Supplemental Fig. 1, Supplemental Table II) (i.e., the fold increase 2× protocol; Supplemental Fig. 1, Supplemental Table I). Stated 0s show unstimulated cells. For specificity experiments, cells were sensitized with donor 2 serum (dust mite and peanut allergic) and desensitized to Der p Ag and challenged with peanut Ag or desensitized to peanut Ag and challenged with Der p Ag.

DNP and NP. WT mBMMCs or Tg hBMMC (50 μl/tube containing either 0.5×10^6 or 1×10^6 mBMMCs) were stimulated with increasing concentrations of DNP-HSA at 10-min intervals at 37°C in 11 incremental doses, starting at 1 pg and reaching 1 ng (or 10 ng) as previously described (7) (Supplemental Table I), and placed on ice. The same method was used for anti-NP IgE sensitization (0.5 mg/10^6 cells/ml) and activation with 10 ng (20 pg/ml) of NP-BSA or control BSA at 10 ng (20 pg/ml) for 10 min. For desensitization, the above protocol of 11 incremental doses was used (starting dose 10 pg, targeting 10 ng total). The total time was 110 min for desensitization. Cell viability was assessed by trypan blue dye exclusion.

Eleven-step activation and desensitization. For experiments evaluating activation, 11 tubes were used, each containing 50 μl/tube of either 0.5×10^6 or 1×10^6 mBMMCs. Each tube received a single dose of Ag in 50 μl, representing each of the 11 steps. Cells were incubated at 37°C for 10 min, placed on ice, and processed for β-hexosaminidase release assay or flow cytometry. For experiments evaluating each step of the desensitization, 11 tubes were used (50 μl/tube containing either 0.5×10^6 or 1×10^6 mBMMCs), the first tube received one dose only, the second tube received two doses (the first dose and, 10 min later, the second dose), and each tube received one more dose than the previous tube up to the last tube, which received 11 doses added sequentially at 10-min intervals at 37°C for a total of 110 min.

3α-Aminocholestane. For selected experiments, mBMMCs were activated and desensitized in the presence of 3α-aminocholestane (3AC), a selective inhibitor of SHIP-1, to block phosphatase activity. The 1×10^6 cells condition was incubated with 10 μM, 15 μM, or 20 μM of 3AC at 37°C (17). After 30 min, cells were washed and resuspended with 50 μl medium and activated or desensitized with 1 ng DNP-HSA or 1 ng HSA control. LAD2 cells were used to assess the effect of 3AC in activation and desensitization of human mast cells. A concentration of 15 μM 3AC or vehicle (200 proof ethanol) was added to 1.5×10^6 cells and incubated for 30 min at 37°C. The cells were washed with sterile HBSS, resuspended in warmed StemPro34 media (prepared as above), and split into three tubes (0.5 million cells in 50 μl) for control, activation, and desensitization conditions. A quantity of 2 μl of lysosomal-associated membrane protein 1 (LAMP-1) Ab (clone H4A3; BioLegend, San Diego, CA) was added to each tube to assess activation and desensitization. The control cells then received 50 μl of warmed media with a final BSA dose of 1 μg. The activation cells received 50μl of warmed media with a final goat anti-human myeloma IgE (polyclonal human; Chemicon) dose of 1 μg. Control and activation conditions were kept at 37°C for 10 min before being placed on ice. The desensitization group was given anti-IgE in warmed media through 11 steps of 10-min incubations each at 37°C for a final dose of 1 μg anti-IgE in 50 μl of warmed media (dose increments match Supplemental Table I, with the only change being the final dose of 1 μg). After the final desensitization step, cells were washed, resuspended in FACS buffer, and collected on the FACSCanto II flow cytometer. Percentage degranulation was reported for the activation and desensitization groups on the basis of gating around 1% of LAMP-1-positive cells in the control condition.

Calcium ionophore. Calcium ionophore (A23187; Sigma-Aldrich) was added to the cell suspension to reach a total volume of 100 μl and a concentration of 8 μM. BMMCs were then activated or desensitized, and β-hexosaminidase was quantified.

β-Hexosaminidase release assay. Activated or desensitized BMMCs were placed on ice, then centrifuged, and cell pellets were lysed by resuspension in culture medium containing 0.5% Triton X-100. β-Hexosaminidase release was assessed by a kinetic microplate ELISA reader (Molecular Devices, Sunnyvale, CA), and percentage release was calculated as described previously (3).

Western blot analysis

Primary Abs used, including SHIP-1 (catalog no. 2728; Cell Signaling Technology); phospho-SHIP-1 (Tyr1020) Ab (catalog no. 3941; Cell Signaling Technology); phospho-Src/Lyn (Tyr416) Ab (catalog no. 2101; Cell Signaling Technology); phospho-Syk (Tyr525/526) Ab (catalog no. 2711; Cell Signaling Technology); phospho-p38 MAPK (Thr180/Tyr182) Ab (catalog no. 9211; Cell Signaling Technology); β-actin Ab (catalog no. 4967; Cell Signaling Technology), and goat anti-rabbit IgG-HRP conjugate (catalog no. 1706515; Bio-Rad Laboratories) BMMCs (1×10^6 cells/condition), were lysed on ice for 20 min in radioimmunoprecipitation assay lysis buffer (100–120 μl/1×10^6 cells). Radioimmunoprecipitation assay lysis buffer (Santa Cruz Biotechnology) was supplemented with 4 mM PMSF 10 μl/ml protease inhibitor mixture, 2 mM sodium orthovanadate, and 10 μl/ml phosphatase inhibitor cocktails A and B (Roche, Santa Cruz Biotechnology). Protein lysates were resuspended with LDS sample buffer 4× (Novex) containing 2.5% 2-ME heated at 70°C for 10 min, and proteins were separated by NuPAGE 4–12% Bis-Tris gels and transferred to a polyvinylidene difluoride membrane or subjected to SDS-PAGE on a 4–12% polyacrylamide gel and transferred to a nitrocellulose membrane (Invitrogen). Membranes were blocked with 3% nonfat dry milk for 1 h at room temperature and probed with primary Abs (1:500 SHIP-1, 1:1,000 p-SHIP-1, 1:500 p-Src/Lyn, 1:300 p-Syk, 1:20,000 p-p38 MAPK, and 1:100,000 β-actin) in 3% BSA/nonfat dry milk overnight at 4°C, washed, and probed with 1:2,000 HRP-conjugated goat anti-rabbit IgG for 4–6 h at room temperature. Signal detection was performed with SuperSignal West Pico Chemiluminescent Substrate (Pierce) and exposed to film. Densitometry and relative expression of bands was quantified using ImageJ software.

Microscopy

Light microscopy with toluidine blue staining. The cytoplasmic and granular morphology of 4–6-wk-old mature WT mBMMCs and 6–8-wk-old mature Tg hBMMCs was assessed by toluidine blue in previously sensitized cells with anti-DNP IgE and anti-NP IgE, which were activated or desensitized with 1 ng and 10 ng of DNP-HSA or NP-BSA and negative control HSA or BSA. After desensitization or activation, cells were washed and resuspended in cold PBS, transferred onto poly-L-lysine-coated round coverslips for 20 min at 4°C, and fixed with 4% paraformaldehyde in PBS for 10 min at 4°C. After three PBS washes, cells were mounted using an aqueous mounting medium (15% w/v polyvinyl alcohol, 33% v/v glycerol, 0.1% azide).

Fluorescence microscopy. mBMMCs sensitized with anti-DNP IgE (1 μg/ml) were challenged and desensitized with DyLight Fluor 649-conjugated DNP (23) in a dark room using 500,000 cells/condition. Because of detection limitations, DNP was 5 ng (10 pg/ml), and the desensitization protocol was adjusted at 5× concentrations (Supplemental Table I). Cells were desensitized with 11 steps starting at 5 pg and targeting 5 ng. After activation or desensitization, cells were placed on ice and centrifuged to remove the supernatant. Cells were washed twice and resuspended in 200 μl cold PBS plus 200 μl of paraformaldehyde 4% during 15 min at room temperature, washed twice with cold PBS, and resuspended in 400 μl of PBS. A quantity of 200 μl (250,000 cells) was transferred to a 12-mm round coverslip for cytospin (10 min at 500 rpm). Coverslips were then transferred to a 24-well plate, cell side facing up, and 500 μl of blocking buffer (10% BSA) was added to each well for 30 min at room temperature. After washing, cells were incubated for 12 h with 5 μl of each Ab (PE anti-mouse LAMP-1 [0.2 mg/ml], red; FITC anti-mouse c-Kit [0.5 mg/ml], green; mouse Fc block purified rat anti-mouse CD16/CD32 [0.5 mg/ml]) in 500 μl of PBS and then washed twice with ice-cold PBS. Images were collected using a KEYENCE BZ-X700 fluorescence microscope (Keyences Corporation).

Actin and tubulin confocal microscopy. After activation or desensitization, WT BMMCs were washed and transferred onto poly-D-lysine (Sigma-Aldrich)-coated chamber slides (Nunc) for 20 min at 4°C. For F-actin staining, cells were fixed with BD Cytofix/Cytoperm solution (BD Biosciences) for 20 min, washed three times with 0.05% PBS-saponin (Merck), incubated with phalloidin-tetramethylrhodamine isothiocyanate following supplier instructions (Sigma-Aldrich) in 0.05% PBS-saponin for 40 min at 4°C, and washed twice with 0.02% PBS-saponin and PBS. For α-tubulin staining, cells were washed and incubated with 0.2% PBS-Tween 20 (Acros Organics) with 5% goat serum (Sigma-Aldrich) and purified rat anti-mouse CD16/CD32 (BD Biosciences). Then, cells were washed with 0.2% PBS-Tween 20 and incubated with anti-α-tubulin (B5-1-2; Sigma-Aldrich) and Alexa Fluor 488 goat anti-mouse IgG (Invitrogen) Ab in 0.2% PBS-Tween 20 containing 1% BSA. Slides were washed twice with 0.2% PBS-Tween 20 and PBS, and coverslips with DAPI mounting medium were added (Vector Laboratories). A 63× objective on a Nikon A1 microscope was used, and the fluorescence intensity was measured as mean Gray value of maximum-projection images using ImageJ software. Four experiments were done as described previously

(29), and 75–100 BMMCs per condition were analyzed. β-Hexosaminidase was assessed for each condition to validate activation and desensitization.

Flow cytometry

Mast cell activation was assessed by measuring LAMP-1 (CD107a) surface expression. LAMP-1 (CD107a) surface expression on Tg hBMMCα was determined by adding 5 μg/ml APC anti-mouse CD107a (clone 1D4B; BioLegend) or 5 μg/ml allophycocyanin rat IgG1a, κ (isotype control, BioLegend) to 50 μl of BMMC suspension before activation or desensitization (Supplemental Table II). Tg hBMMCα were placed on ice 10 min after stimulation and washed with ice-cold FACS buffer (PBS 1× containing 0.5% BSA and 0.1% sodium azide). Cells were then washed with ice-cold FACS buffer and stained for 30 min on ice: for Tg hBMMCs, 2.5 μg/ml PE anti-human IgE (clone MHE-18; BioLegend) or 2.5 μg/ml PE mouse IgG1, κ (isotype control; BioLegend) and 10 μg/ml FITC anti-human FcεRIα (clone AER-37; BioLegend) or 10 μg/ml FITC mouse IgG2b, κ (isotype control, BioLegend); for WT mBMMCs, 5 μg/ml APC anti-mouse CD107a (clone 1D4B; BioLegend) or 5 μg/ml APC rat IgG1a, κ (isotype control; BioLegend), 5 μg/ml FITC anti-mouse IgE (clone RME-1; BioLegend) or 5 μg/ml FITC rat IgG1, κ (isotype control; BioLegend) and 2 μg/ml PE anti-mouse FcεRIα (clone MAR-1; BioLegend) or 2 μg/ml PE anti-mouse LILRB4 (clone H1.1) or 2 μg/ml PE Armenian hamster IgG (isotype control; BioLegend). Activated, desensitized, or HSA-treated mBMMCs were first washed and resuspended in ice-cold 1× PBS containing 0.5% BSA and 0.05% sodium azide (FACS buffer) and then incubated for 10 min on ice (4°C) with either anti-FcγRI/II mAb (eBioscience) or 1 μg/ml anti-mouse CD16/32 (TruStain fcX, FcγRIII; BioLegend) to block Fcγ receptors. Cells were then washed with ice-cold FACS buffer and incubated on ice with FITC anti-mouse FcεRIα Ab clone MAR-1 0.5 mg/ml, Brilliant Violet 510 anti-mouse CD117 (c-Kit) Ab clone 2B8 0.2 mg/ml, PerCP/cyanine 5.5 anti-ERK1/2 phospho-Thr202/Tyr204 Ab clone 6B8B69 (BioLegend), PE mouse anti-SHIP-1 clone 32/SHIP-1 0.2 mg/ml (BD Biosciences), rabbit anti-Syk (tyrosine protein kinase SYK, spleen tyrosine kinase) (Pacific Blue) clone D3Z1E 2 mg/ml (US Biological Life Sciences), and allophycocyanin phospho-Syk (Tyr348) mAb (clone moch1ct) 5 μl (0.06 μg)/test (eBioscience), or with the recommended isotype controls (FITC Armenian hamster IgG isotype control Ab, clone HTK888, 0.5 mg/ml), Brilliant Violet 510 rat IgG2b, κ isotype control Ab (clone RTK4530, 0.2 mg/ml), PerCP/cyanine 5.5 mouse IgG2a, κ isotype control Ab (clone MOPC-173, 0.2 mg/ml) (BioLegend), PE mouse IgG1, κ isotype control (clone MOPC-21, 0.2 mg/ml) (BD Biosciences), mouse IgG1 κ isotype control (clone P3.6.2.8.1, 0.2 mg/ml), APC (eBioscience) for 30 min at 4°C. Samples were read on a BD FACSCanto (BD Biosciences) or BD LSR Fortessa (BD Biosciences) flow cytometer using FACSDiva acquisition software, and data were analyzed in FlowJo analysis software (BD Biosciences, Ashland, OR).

SHIP-1 knockdown with siRNA

Prior to sensitization, BMMCs were electroporated with an Amaxa Nucleofector II according to the manufacturer's instructions (Amaxa; Lonza). BMMCs were divided into four groups: nonelectroporated (NE), blank electroporation (B), electroporation with anti-SHIP-1 siRNA (S) (anti-SHIP1 siRNA 7), or electroporation with scrambled negative control siRNA (NC). The anti-SHIP1 siRNA used was against mouse inositol polyphosphate-5-phosphatase D (Mm_Inpp5d_7 FlexiTube siRNA) with detected transcripts: NM_001110192 (4937 bp), NM_001110193 (4757 bp), NM_010566 (4940 bp). For all groups, 1.2×10^6

A

Antigen: DNP-HSA/BSA

Steps	Time (min)	Volume* (μL)	Concentration in added volume (pg/ μL)	Final Concentration (in treated tube**) (pg/μL)	Dose (pg)	Volume* (μL)
1	0	1	1	0.02	1	4
2	10	1	5	0.1	5	4
3	20	1	5	0.2	5	4
4	30	1	10	0.4	10	4
5	40	1	10	0.6	10	4
6	50	2	10	0.9	20	5
7	60	2	20	1.5	40	5
8	70	4	20	2.7	80	5
9	80	8	20	4.7	160	5
10	90	16	20	7.5	320	5
11	100	17.5	20	9.6	350	5
11 steps	110 min	54.5 μL			1 ng	50 μL

*added to 50 μL BMMCs; ** after dose added to cell suspension

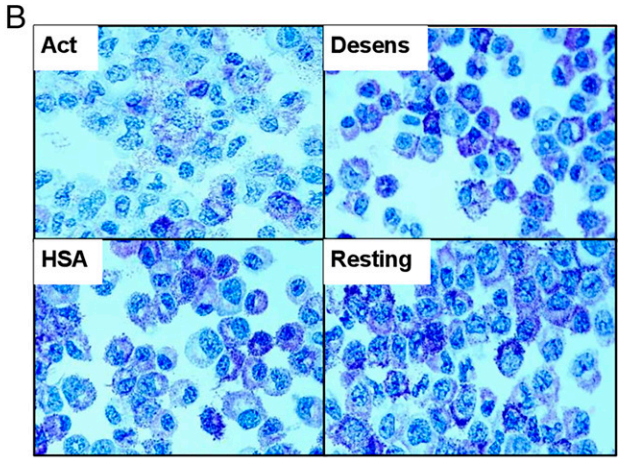

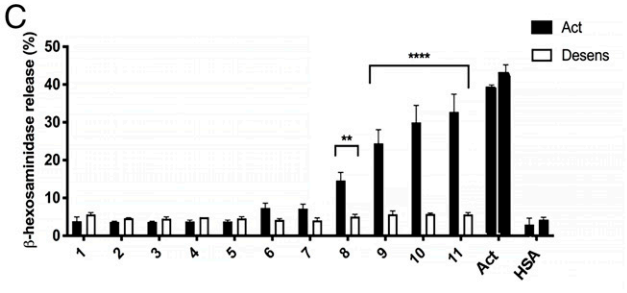

FIGURE 1. Desensitization of mBMMCs induces significantly less β-hexosaminidase and maintains granule integrity. (**A**) Desensitization protocol adapted from Sancho-Serra et al. (3). After overnight sensitization with anti-DNP IgE, 11 doses of DNP-HSA were delivered sequentially to 1×10^6 BMMCs at 10-min intervals until the target dose of 1 ng for DNP-HSA was reached. For activation and HSA control, single doses were delivered to 1×10^6 BMMCs in separate tubes. (**B**) WT mBMMCs were sensitized with anti-DNP IgE (1 mg/ml). Clockwise from the top left: activated (Act) with 1 ng DNP-HSA; desensitized (Desens) to 1 ng DNP-HSA; treated with 1 ng HSA or untreated (resting). Representative images of $n = 6$ independent experiments with toluidine blue at ×100 magnification. (**C**) WT mBMMCs were sensitized with 0.25 μg anti-DNP IgE (per 10^6 cells/ml). The percentage of β-hexosaminidase release was calculated at each step of the 11 steps of the desensitization and corresponding activation doses. For desensitization, each step represents an additional number of doses delivered every 10 min up to 11 doses in 110 min, and for activation, each step is a single dose. The positive control was cells activated with a single 1-ng DNP-HSA dose (Act), and the negative control was 1 ng HSA, and processed at 10 and 110 min. Mean with SEM of $n = 5$ independent experiments. $^{**}p < 0.01$, $^{****}p < 0.0001$.

BMMCs were resuspended in 92 μl of Nucleofector solution kit T. The remaining 8 μl varied, depending on the group: group NE received 8 μl of Nucleofector solution, group B received 8 μl of Nucleofector solution, group S received 8 μl of 1 nM anti-SHIP1 siRNA (catalog no. SI04919726; QIAGEN), and group NC received 8 μl of 1 nM AllStars negative control siRNA (catalog no. SI03650318; QIAGEN). Cells were electroporated using program T-030, except NE cells, incubated for 5 d for maximal SHIP-1 knockdown, and flow cytometry, Western blot, or β-hexosaminidase release assays were performed as described above.

Deletion of SHIP-1 in Cre SHIP-1 fl/fl BMMCs

Cells were isolated and cultured from bone marrow from Cre SHIP-1 fl/fl mice (gift of William Kerr laboratory, SUNY Upstate Medical University, Syracuse, NY) as per WT BMMC protocol in RPMI medium with 10% FBS in 10 ng/ml IL-3 for 4 wk. Mature Cre SHIP1 fl/fl BMMCs were incubated with TatCre recombinase (MilliporeSigma) to catalyze the site-specific deletion of SHIP-1 between the two flox sites. A total of 3 million SHP-1 Cre^+ BMMCs were split into two wells of 1.5 ml media (R10/supplemented RPMI, 1% penicillin-streptomycin, 10 ng/ml rmIL3) each, with 2.7 μM TatCre recombinase (EMD Millipore) added to one well. After 24-h incubation at 37°C, the cells were collected, washed with HBSS, and resuspended in 1.5 ml of warmed media. Cells were then sensitized with 1 μg/ml anti-DNP IgE (clone SPE-7; Sigma-Aldrich) for 48 h at 37°C before they were collected, washed with HBSS, resuspended in warmed media, and split into tubes for activation, desensitization, and control groups (as described previously; Supplemental Table I). A quantity of 2 μl LAMP-1 was added to each sample for the duration of activation, control, or desensitization. After 10 min on ice, cells were fixed, permeabilized, and stained intracellularly for SHIP-1.

Statistical analysis

GraphPad Prism 8.0 software was used to perform all statistical tests (GraphPad Software, La Jolla, CA). For all experiments, groups were analyzed using unpaired, two-tailed Student *t* tests, where $*p < 0.05$, $**p < 0.01$, and $***p < 0.001$ were used to determine statistical significance. The data shown in all graphs are represented as mean ± SEM.

Results

Rapid IgE desensitization inhibits β-hexosaminidase release while preserving granule integrity in mouse BMMCs

We reproduced the Sancho-Serra et al. and Morales et al. (3, 15) protocol for IgE activation and desensitization of BMMCs with 11 doses of DNP-HAS starting at a concentration of 0.02 ng/ml (Fig. 1A–C). Activated cells received one dose of Ag at each step, whereas desensitized cells received the summation of previous steps (Fig. 1A). Desensitized cells remained fully granulated after receiving the target dose of 1 ng in 11 steps, whereas activated cells with the same dose presented extensive degranulation with empty cytoplasm (Fig. 1B). With the first seven doses of activation and desensitization, whereas 9.1% of the target dose was delivered, the percentage of β-hexosaminidase release was not different from the control HSA/BSA (Fig. 1C). From steps 8 to 11, activated cells presented an incremental dose response, whereas desensitized cells remained insensitive to the increments in cumulative doses, indicating uncoupling of signal transduction (Fig. 1C). Suboptimal sequential Ag doses added during the first seven desensitization steps segregated crosslinked FcεRI receptors from activation partners. We next examined inhibitory signals generated by changing the starting dose, the interval time between doses, and the dose increase at each step.

Transgene hBMMCα desensitization with dust mites and peanut allergens is specific and depends on the starting dose, rate of allergen increases, and time between doses

To provide evidence of the universal application of desensitization, we used Tg hBMMCs sensitized with human allergic serum and activated with dust mites and peanut allergens. A dose–response release

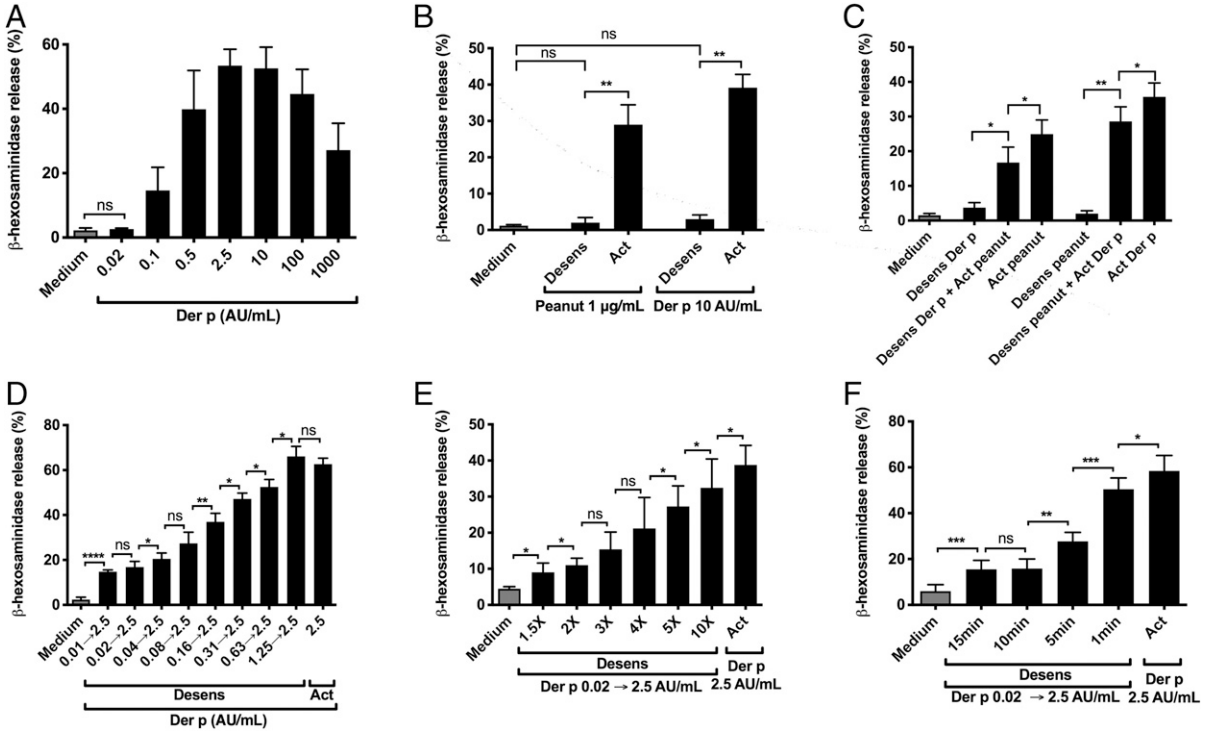

FIGURE 2. Desensitization of Tg hBMMCα is Ag specific and depends on starting Ag dose, rate of dose increases, and time between steps. Percentage β-hexosaminidase release was calculated in Tg hBMMCα sensitized with serum from a dust mite and peanut allergic donor (**A**–**C**) or a dust mite allergic donor (**D**–**F**) and activated with Der p or peanut allergens (Supplemental Fig. 1 and Supplemental Tables I–IV) at 10-min intervals (A–E) or variable time intervals (F). (A) Single dose–response activation for Der p allergen with optimal plateau doses. (B) Activation and desensitization to peanut (target dose 1 μg/ml) and Der p (target dose 10 AU/ml) allergens. (C) Der p desensitized hBMMCα stimulated with an activating dose of peanut, and peanut desensitized hBMMCα stimulated with an activating dose of Der p to show specificity. (D) Desensitization to Der p 2.5 AU/ml with varying starting concentrations (Supplemental Fig. 1, Supplemental Table II). (E) Desensitization to Der p 2.5 AU/ml with varying concentration increases per step (Supplemental Fig. 1, Supplemental Table I). (F) Desensitization to Der p 2.5 AU/ml with varying time intervals between steps (Supplemental Figure 1, Supplemental Table III). 1 AU = 0.0025 μg/ml or 2.5 ng/ml of Derp 1. Mean with SD of four independent experiments. $*p < 0.05$, $**p < 0.01$, $***p < 0.001$, $****p < 0.0001$.

of β-hexosaminidase was seen in Tg hBMMCs sensitized with human dust mite allergic serum when activated with Der p with an optimal activation at 2.5 AU/ml and a plateau at 10 AU/ml (Fig. 2A). Tg hBMMCs were then sensitized with human serum containing dust mites and peanut IgE and activated and desensitized with dust mites and peanut Ags (Supplemental Fig. 1). Desensitization to Der p and to peanut allergens in 11 doses significantly inhibited β-hexosaminidase release (Fig. 2B) as compared with activation. Specific desensitization was shown because Tg hBMMCs desensitized to dust mites partially inhibited β-hexosaminidase release when activated by peanut allergen and Tg hBMMCs desensitized to peanut partially inhibited activation by dust mite allergens (Fig. 2C). Dust mite Ag Der p was used to establish the optimal starting dose, dose increments, and time between doses (Supplemental Tables I–IV). Maximal inhibition of β-hexosaminidase release was observed when the starting concentration was 100 times lower than the target concentration (Fig. 2D), with twofold or less increases per step (Fig. 2E) and when doses were delivered at least 10 min apart (Fig. 2F). We then assessed the dynamic membrane changes associated with desensitization by following LAMP-1 and membrane receptors.

Reverse surface expression of LAMP-1, hFcεRIα, and hIgE during activation and desensitization

LAMP-1 is translocated from the cytoplasm to the surface membrane during activation and is associated with the release of granule mediators (30). We followed LAMP-1 to assess the dynamic membrane changes associated with desensitization. LAMP-1 translocation to the membrane was maximal with 2.5 AU/ml delivered as a single activating dose (Fig. 3A, 3D, lower right panel) and was negligible in cells desensitized to Der p starting at 0.02 AU/ml and reaching 2.5 AU/ml (Fig. 3A, 3D, upper right panel). Increased translocation was seen with increasing starting doses (Fig. 3A), mirroring the release of β-hexosaminidase (Fig. 2D). In contrast, the surface expression of IgE (Fig. 3B) and FcεRIα (Fig. 3C) decreased maximally with activation, indicating internalization, and minimally with desensitization, indicating surface membrane retention. Cells desensitized with a starting concentration of 0.02 AU/ml (1% of target) and a target dose of 2.5 AU/ml did not express LAMP-1 and remained hIgE/hFcεRIα positive, in contrast to cells activated with 2.5 AU/ml, which expressed LAMP-1 and became hIgE/hFcεRIα negative (Fig. 3D and 3E, upper right panel for desensitization and lower right panel for activation). Starting desensitization at a concentration of 0.16 AU/ml (6.4% of target concentration) induced partial expression of LAMP-1 and a reduction in the surface expression of FcεRI and IgE (Fig. 3D and 3E, lower left panels), indicating internalization and a decrease in desensitization. The reverse movements of LAMP-1, hIgE, and FcεRI during activation and desensitization to the same target dose were consistent with a dynamic association with divergent downstream partners induced by cumulative doses during desensitization versus single doses during activation. To assess the impact of desensitization, we looked at its specificity, the potential depletion of mediators, and membrane receptor changes.

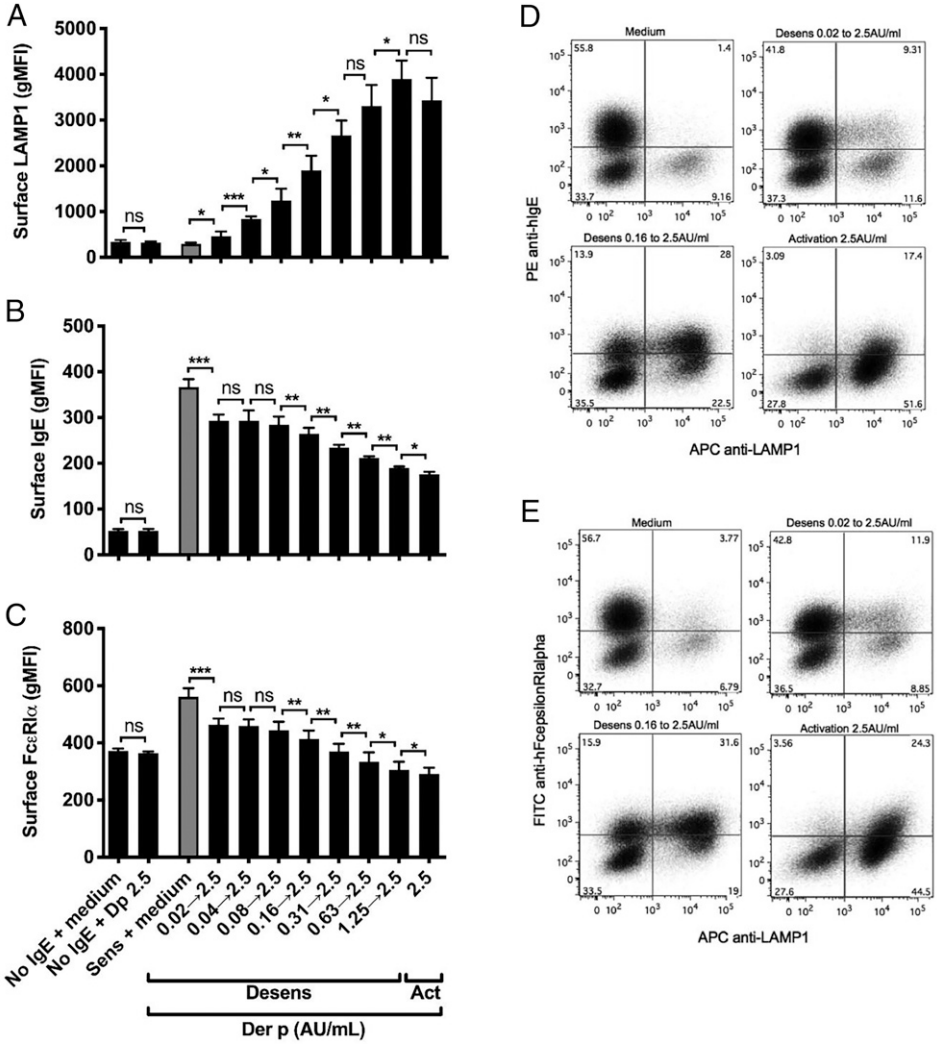

FIGURE 3. Surface expression of LAMP-1 is decreased by desensitization while IgE and FcεRIα remain at the cell surface. (**A**–**C**) Surface expression by quantitative flow cytometry analysis (geometric mean fluorescence intensity [MFI]) of LAMP-1, IgE, and FcεRIα, respectively, on Tg hBMMCα sensitized (or not) with serum from a dust mite allergic subject and subsequently desensitized or activated with Der p 2.5 AU/ml. Desensitization was performed with increasing starting concentrations of Der p as in Fig. 2E. (**D** and **E**) Dot plot of surface expression of LAMP-1, IgE, and FcεRIα on Tg hBMMCα sensitized with serum from a dust mite allergic subject and treated with medium, desensitized with Der p 2.5 AU/ml starting at 0.02 AU/ml or 0.16 AU/ml, or activated with Der p 2.5 AU/ml. Mean with SD of $n = 4$ experiments, where $*p < 0.05$, $**p < 0.01$, $***p < 0.001$.

Desensitized mBMMCs are refractory to activation and cannot internalize Ags and surface receptors but are not depleted of granule mediators

We looked at the movements of activating receptors such as KIT, which has been shown to amplify IgE-mediated signals (31), and inhibitory receptors such as gp49B and PDL-1, which have been shown to compete with IgE-mediated signals (22) to assess membrane changes beyond FcεRI. gp49B1, PDL-1, and KIT were internalized during activation (Fig. 4A) but remained at the cell surface during desensitization, in contrast to LAMP-1 but similar to the fate of IgE and FcεRI (Fig. 3A–3C), indicating that membrane changes during desensitization extended beyond Ag/IgE/FcεRI aggregates. Desensitized cells challenged with an optimal Ag dose remained hyporesponsive (Fig. 4B), indicating a prolonged inhibitory state, which was not due to the depletion of mediators, because the response to calcium ionophore A23187 was intact (Fig. 4C). Calcium ionophore A23187 complexes with extracellular calcium and allows intracellular entry, bypassing membrane receptors, through a non-IgE associated mechanism (32). To follow simultaneous membrane changes during desensitization, fluorescent labels were used (Fig. 4D and 4E). LAMP-1 (red) was detected at the cell surface of activated cells, but not on desensitized cells, and KIT (green) was detected in desensitized and resting cells, but not on activated cells (Fig. 4E). DNP-BSA Ag (purple) was internalized during activation but remained at the cell surface in desensitized and resting cells. These opposite changes correlated with changes observed with toluidine blue showing extensive degranulation in activated cells, but not in desensitized cells (Fig. 4D), and with the inhibition of β-hexosaminidase release during desensitization (Fig. 4F). Because membrane changes and the release of mediators depend on actin and tubulin movements, we analyzed the impact of desensitization on actin and tubulin protein polymerization.

Tubulin and actin movements are limited in desensitized mBMMCs

FcεRI activation by multimeric Ags induces an increase in microtubule structures of α- and β-tubulin heterodimers and the disassembly of the cortical F-actin rings (33, 34). We observed the formation of cortical αβ-tubulin microtubules in activated cells, which was significantly inhibited in desensitized cells as compared with resting and HSA-activated cells (Fig. 5A, 5C). Concomitant disassembly of

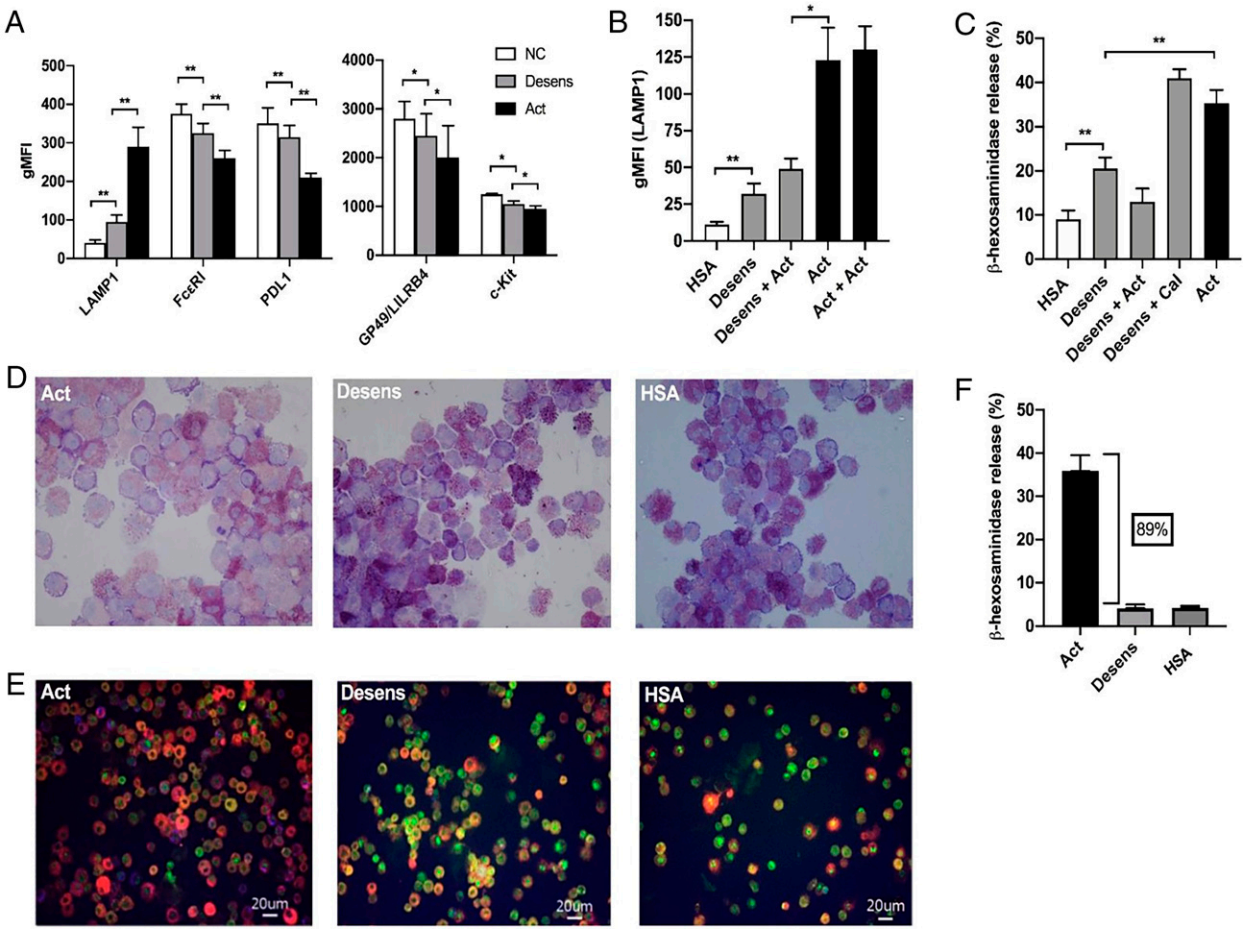

FIGURE 4. Desensitization prevents internalization of Ags and surface receptors KIT, gp49B1, and PDL1 and does not deplete mediators in mBMMCs. WT mBMMCs were sensitized with anti-DNP IgE and activated or desensitized with DNP-HAS. (**A**) Quantitative surface expression (geometric mean fluorescence intensity [gMFI]) of LAMP-1, FcεRI, PDL1, GP49B1/LILRB4, and KIT was measured by flow cytometry after activation and desensitization to 1 ng DNP-HSA. NC, negative control (HSA). (**B**) LAMP-1 expression (gMFI) after activation or desensitization and after desensitized mBMMCs were challenged with an additional dose of 1 ng DNP-HSA. (**C**) Percentage β-hexosaminidase (β-hex) release after mBMMCs were desensitized and treated with either 1 ng of DNP-HSA or calcium ionophore (CaI). (**D**) Light microscopy of Tg hBMMCs. Anti-NP IgE-sensitized Tg hBMMCs were activated (Act) or desensitized (Des) with 10 ng of NP-BSA (adapted from Fig. 1A for Ag dose ×10) or treated with HSA and stained with toluidine blue (original magnification ×63). (**E**) Fluorescence microscopy of mBMMCs sensitized with anti-DNP IgE and activated (Act) and desensitized (Desens) with 5 ng of DyLight Fluor 649-conjugated DNP or HSA. Color legend: red, PE anti-mouse LAMP-1; green, FITC anti-mouse c-Kit; purple, DyLight Fluor 649-conjugated DNP (original magnification ×40). (**F**) Percentage β-hexosaminidase released after activation or desensitization with 10 ng NP-BSA or 10 ng HSA. $*p < 0.05$, $**p < 0.01$, $***p < 0.001$.

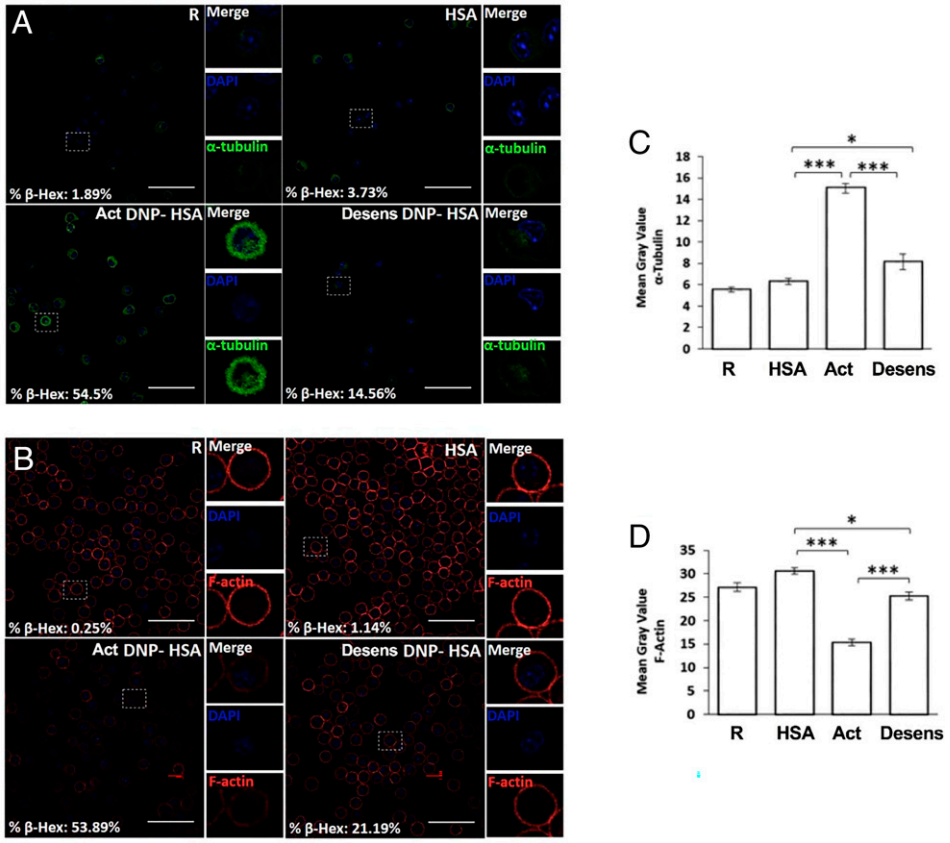

FIGURE 5. α-Tubulin and F-actin movements are halted during desensitization of mBMMCs. (**A** and **B**), Confocal images of mBMMCs stained with anti-tubulin (green) (A) or with Rh-Phalloidin (red) (B) for F-actin detection. High magnification at right. Scale bars, 50 μm. % β-Hex, % β-hexosaminidase; Act, activated mBMMCs; Desens, desensitized mBMMCs; HSA, control IgE-sensitized mBMMCs; R, resting mBMMCs. Representative pictures of one of two independent experiments. (**C**) Quantification of α-tubulin and (**D**) F-actin staining by confocal microscopy, analyzed using ImageJ software. Values indicate mean ± SEM ($n = 75–100$). *$p < 0.05$, ***$p < 0.001$. Representative data of one of two independent experiments.

cortical F-actin occurred during activation, which was significantly inhibited during desensitization as compared with resting and HSA-activated cells (Fig. 5B, 5D). Desensitization promoted the stabilization of the cytoskeleton, limiting the movements of actin and tubulin without significant disassembly of F-actin and little formation of microtubules, likely contributing to membrane reorganization, which has been previously described and attributed to aberrant actin remodeling (1). Because activation-induced cytoskeletal changes associate with FcεRI-induced signal transduction, we investigated the activation and phosphorylation of Syk, p38-MAPK, and SHIP-1 proteins.

Phosphorylation of Syk, Lyn, p38-MAPK, and SHIP-1 is increased in activated mBMMCs and decreased in desensitized mBMMCs

Aggregation of FcεRI receptors with optimal Ag results in upstream phosphorylation of β- and γ-chain ITAMs, Lyn activation, docking and phosphorylation of Syk through its two SH2 domains, and activation of enzymes and adapter molecules, leading to extracellular calcium influx and mediator release. Downstream events include the phosphorylation of p38-MAPK, which regulates nuclear transcription factors and the generation of cytokines (12, 35). Syk phosphorylation was found to be dose dependent following single activation doses of DNP-HSA (Fig. 6A). In contrast, when delivering the target dose in sequential increments in desensitization, decreased Syk and p38-MAPK phosphorylation was seen (Fig. 6B). DNP-HSA-activated mBMMCs had high Syk and p38-MAPK phosphorylation, which was significantly reduced in desensitized and HSA-activated cells (Fig. 6C, 6D), suggesting the downstream uncoupling of signal transduction. Surprisingly, SHIP-1, which has been shown to counteract Syk activation (36), was less phosphorylated in desensitization than in activation (Fig. 6E, 6F). To further understand these changes, we looked at the dynamic changes at each of the 11 steps of desensitization and corresponding activation doses.

Enhanced phosphorylation of SHIP-1 in the early steps of desensitization. The phosphorylation of Syk, Lyn, p38-MAPK, and SHIP-1 increased with increasing activating doses, which correlated with the observed increases in β-hexosaminidase release (Fig. 7A and Fig. 1A). In contrast, during desensitization, phosphorylation of SHIP-1 was significantly enhanced in the first four steps (Fig. 7B, 7C, and Supplemental Fig. 3A, 3B), whereas Lyn, Syk, and p38-MAPK had no significant increase in phosphorylation. Early phosphorylation of SHIP-1 when β-hexosaminidase release was absent (Fig. 1A) was intriguing, implicating SHIP in the uncoupling of activation signals through an unknown interaction of one of its motifs (18). The NPXY domain functions include protein–protein associations with adaptor proteins, the cytoskeleton, actin, and tubulin, among others (37). To further understand the role of SHIP-1 in desensitization, we blocked its phosphatase function and silenced the protein.

Desensitization does not depend on SHIP-1 phosphatase function and is impaired by SHIP-1 protein silencing. The phosphatase activity of SHIP-1 depletes membrane lipids of phosphatidylinositol (3,4,5)-trisphosphate and prevents the activation of BTK, Akt/PKB, and the influx of extracellular calcium necessary for signal transduction. We wanted to explore if SHIP-1 phosphatase activity could be affected by early SHIP-1 phosphorylation (18) and used 3AC, a cell-permeable steroidal compound that inhibits SHIP-1 catalytic polyphosphatase activity, at doses that have previously been shown not to be cytotoxic (17). Desensitization was not significantly inhibited by the lack of SHIP-1 phosphatase function (Fig. 8A, 8B) in mouse BMMCs or human LAD2 cells, prompting a further look at other SHIP-1

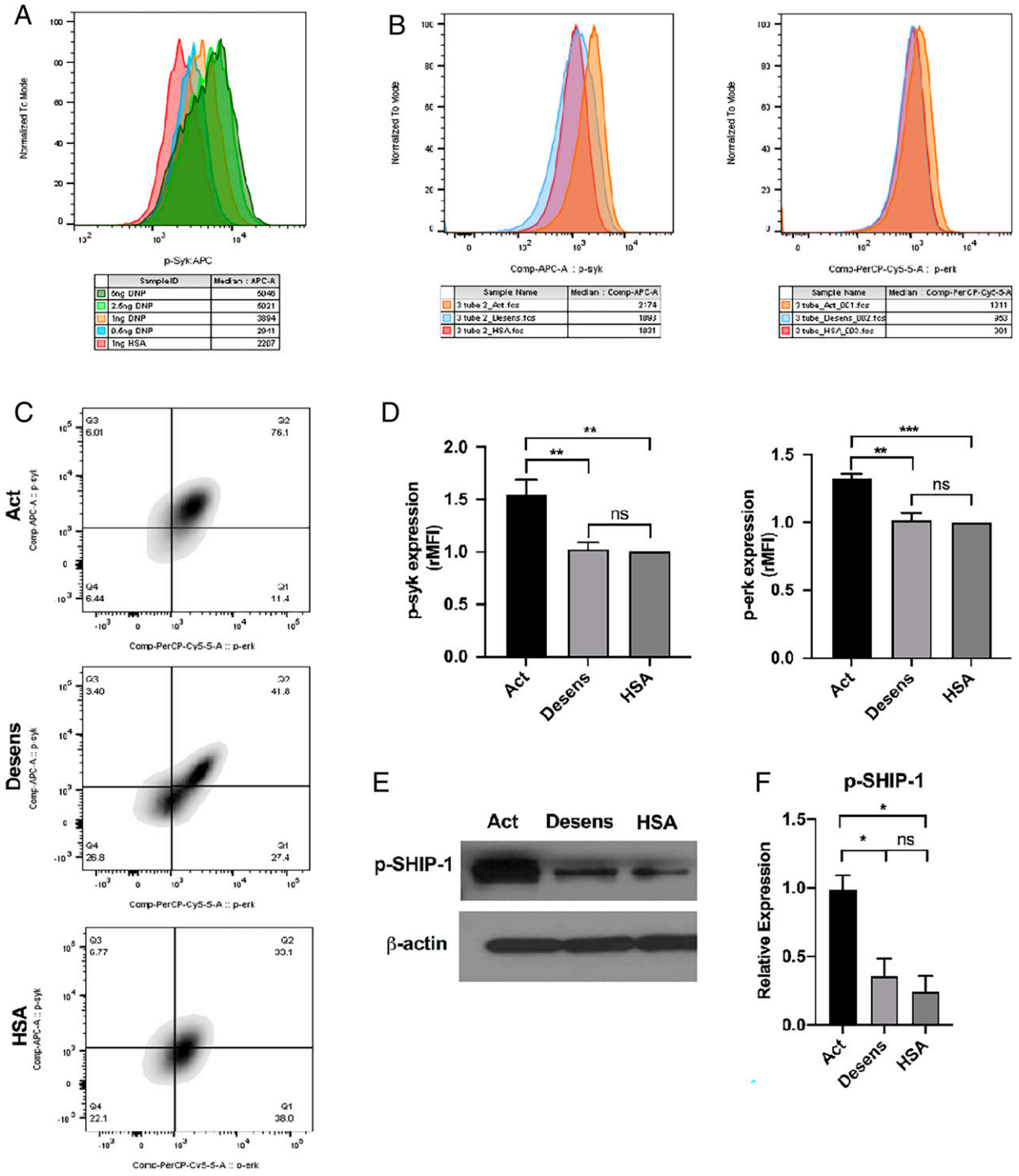

FIGURE 6. Increased phosphorylation of Syk, p-38-MAPK, and SHIP-1 following activation and decreased phosphorylation following desensitization of mBMMCs. (**A**) Flow cytometry of phospho-Syk (p-Syk) expression for sensitized and permeabilized mBMMCs challenged with increasing doses of DNP-HSA after gating on FcεRIα and c-Kit (CD117) double-positive cells (Supplemental Fig. 2). (**B**) Flow cytometry of p-Syk and p-Erk (p38 MAPK/ERK) in permeabilized mBMMCs activated (Act) or desensitized (Desens) with 1 ng DNP-HSA or with 1 ng HSA. (**C**) Flow cytometry density plots of p-Syk versus p-Erk (p38 MAPK/ERK) in activation (Act), desensitization (Desens), and HSA-treated BMMCs. (**D**) Relative median fluorescence intensity (rMFI) of p-Syk (APC) and p-Erk (p38 MAPK/ERK) PerCP-cyanine 5.5 expression in activated (Act), desensitized (Desens), and control (HSA) BMMCs. $n = 7$ and $n = 4$ experiments, respectively, are shown as mean with SEM. $^{*}p < 0.05$, $^{**}p < 0.01$, $^{***}p < 0.001$. (**E**) Western blot showing SHIP-1 phosphorylation (p-SHIP-1) in BMMCs after activation (Act) and desensitization (Desens) with 1 ng DNP-HSA and challenge with 1 ng HSA. Representative of $n = 3$ experiments. (**F**) Relative expression of p-SHIP-1 from (E), $n = 3$, for activation (Act), desensitization (Desens), and HSA-treated BMMCs.

functions through the silencing of SHIP-1 protein using siRNA. siRNA was able to efficiently silence SHIP-1 protein (Fig. 8C, 8D). Activation of BMMCs lacking SHIP-1 was increased as previously reported for SHIP-1-knockout mast cells, although it did not reach total significance between cells transfected with control siRNA and cells transfected with anti-SHIP-1 siRNA ($p = 0.08$) (Fig. 8E) (18). In contrast, cells lacking SHIP-1 had no significant decrease in β-hexosaminidase after desensitization (Fig. 8E, 8F). Because

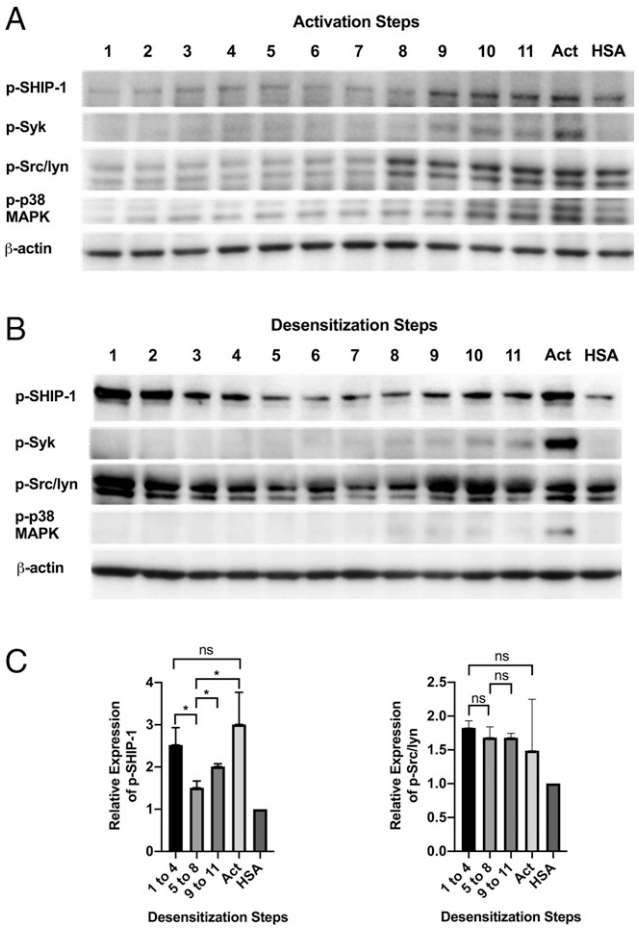

FIGURE 7. Differential phosphorylation of SHIP-1 during activation and early steps of desensitization. (**A**) mBMMCs were sensitized and activated with single doses of DNP-HSA up to 1 ng with 11 total steps (protocol in Fig. 1A) or (**B**) desensitized with incremental doses of DNP-HSA up to 1 ng total in 11 steps (protocol in Fig. 1A). For activation, each tube received one single dose, and for desensitization, each tube received one more dose than the previous one, up to 11 doses in tube 11, at 10 min each dose (110 min total). mBMMCs were activated with one dose of 1 ng DNP-HSA (Act) and with 1 ng HSA. Phosphorylated proteins p-SHIP-1, p-Syk, p-Src/Lyn, and p-Erk (p38 MAPK) were assessed by Western blot analysis probing during each of the steps. (**C**) Steps 1 to 4, 5 to 8, and 9 to 11 (B and Supplemental Fig. 3 A and B) were analyzed for the relative expression of p-SHIP-1 and p-Src/Lyn by densitometry. $n = 3$ experiments where $^*p < 0.05$.

SHIP-1 protein was significantly decreased, as shown in Fig. 8C and 8D in cells electroporated with anti-SHIP-1 siRNA, the lack of SHIP-1 protein was associated with a decrease in desensitization and lack of inhibitory mechanisms, leading to the increase in β-hexosaminidaserelease. We confirmed these results using Cre SHIP-1 flox/flox BMMCs, which were floxed with Tat and presented efficient SHIP-deletion (Supplemental Fig. 4), with significant decrease in SHIP-1 protein. Cells lacking SHIP-1 protein had increased activation and were inefficient at blocking β-hexosaminidase release during desensitization (Fig. 8G, 8H), indicating that SHIP-1 had a central role in multistep desensitization.

Discussion

This study confirms and extends the notion that mast cell IgE multistep desensitization generates and promotes inhibitory signals initiated by FcεRI crosslinking with suboptimal Ag, which requires SHIP-1. Membrane and cytoskeletal movements are blocked (Figs. 4 and 5), and interference in the phosphorylation of upstream targets leads to uncoupling from downstream events (Figs. 6 and 7). Ag–IgE–FcεRI complexes are not internalized as well as membrane receptors KIT, PDL-1, and gp49 (Fig. 4), indicating a structural membrane resistance to outside-in movements, likely due to segregated Ag-specific inhibitory domains, excluding activation partners.

The conditions for multistep desensitization established in this study are independent of allergen and IgE specificity and likely applicable to all inhalant, food, and drug allergens. Desensitization to DNP, NP, dust mites, and peanut Ags is achieved when the starting dose is 1/100 the target dose and doubling suboptimal doses are delivered at 10-min intervals (Figs. 1C, 2B, and 2D–2F) until reaching the target dose. When over 9% of the target dose is delivered in seven steps (Fig. 1C), cells become refractory to activating doses, preserving intact granules (Fig. 1B). Starting at higher doses, decreasing the number of steps and the time interval leads to significant increases in β-hexosaminidase release, with progressive loss of desensitization. No depletion of mediators occurs during desensitization (Fig. 4C), indicating a lack of mediator leakage induced by suboptimal Ag. Desensitized cells cannot be activated with optimal allergen, indicating a dynamic prolonged inhibitory state (Fig. 4B). Significant cross-desensitization is not observed (Fig. 2C), indicating that global cell unresponsiveness is not generated; hence, in a patient allergic to both dust mites and peanut allergens, anaphylaxis after peanut ingestion would be expected while desensitized to dust mites (38).

Because earlier reports had implicated SHIP-1 in the control of mast cell activation and FcεRI signaling (36, 39), we explored its role by looking at its phosphorylation, we blocked its enzymatic phosphatase activity, and we knocked down its protein expression using two different techniques. SHIP-1 tyrosine phosphorylation increased with single activating doses along with the phosphorylation of Lyn, Syk, and p38-MAPK (Fig. 7A) and with the release of β-hexosaminidase, indicating that SHIP-1 tyrosine phosphorylation is associated with a decrease in its phosphatase activity, as others have shown (40). In contrast, SHIP-1 phosphorylation was seen in early desensitization when sequential suboptimal Ag doses were delivered at steps 1 to 4 (Fig. 7B), when there was no release of β-hexosaminidase and when Syk, Lyn, and p38-MAPK were not phosphorylated, indicating a divergent inhibitory function. Blocking its phosphatase activity with 3AC in mouse BMMCs and human LAD2 cells did not abrogate desensitization, indicating that the phosphatase function was not required, regardless of the mast cell origin (Fig. 8A, 8B). To assess nonphosphatase inhibitory functions, we silenced SHIP-1 protein with siRNA and CreSHIP-1 fl/fl BMMCs and were able to significantly lift the block on the inhibition of β-hexosaminidase release, providing evidence of desensitization interference (Fig. 8E–8H). Because the initial steps of desensitization provided suboptimal Ag, we hypothesize that inhibitory iITAMs (41) with monophosphorylated tyrosines are generated in the β- and γ-chains of the crosslinked FcεRI, becoming docking sites for SHIP-1, which contains one SH2 domain, and excluding Syk with two SH2 domains (37). Progressive engagement of the iITAMs by SHIP-1 with increasing suboptimal doses in the first four steps induced transient tyrosine phosphorylation of SHIP-1, allowing interactions with inhibitory partners and likely creating Ag-specific membrane segregated domains. The amino terminal SHIP-1 SH2 domain can bind to phosphotyrosine residues on ITAMs and immunoreceptor tyrosine-based inhibition motifs, and gp49B1 (37) could be recruited by phosphorylated SHIP-1, protecting desensitized FcεRI aggregates from activating partners. B- and γ-chain iITAM would generate membrane proximal traps for SHIP-1, modifying the membrane arrangements around crosslinked FcεRI and changing the configuration of CRAC calcium channels, preventing extracellular calcium entry. Phosphorylated SHIP-1 could bind actin and tubulin, preventing polymerization. At optimal Ag doses, the segregated,

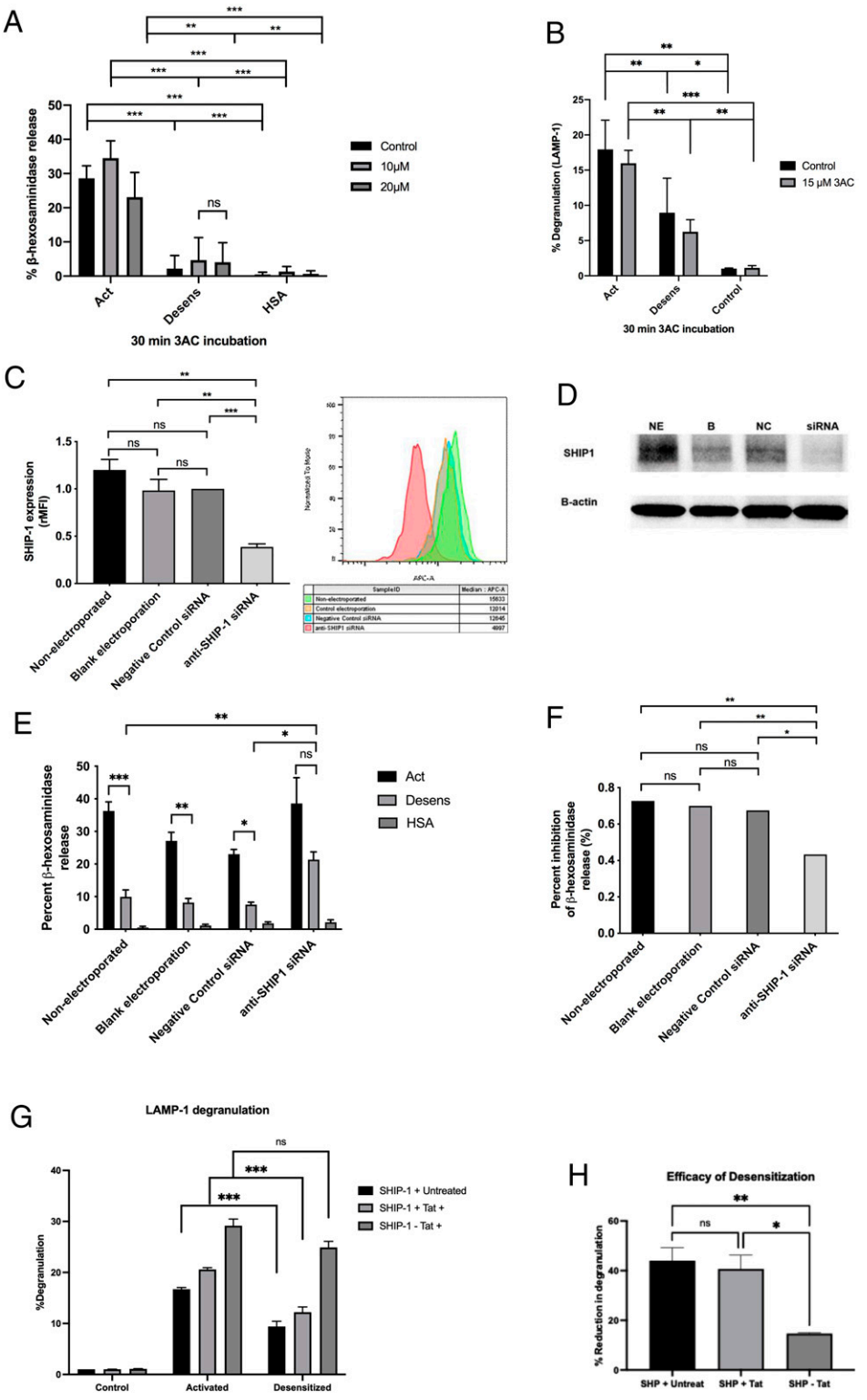

FIGURE 8. SHIP-1 phosphatase function does not impact desensitization, but silencing SHIP-1 protein impairs desensitization in mBMMCs. (**A**) mBMMCs and (**B**) LAD2 cells were sensitized, incubated with 10 μM, 15 μM, or 20 μM of 3AC or vehicle control at 37°C for 30 min, and β-hexosaminidase was measured for activation (Act) or desensitization (Desens) with 1 ng DNP-HSA or 1 ng HSA. $n = 3$ independent experiments. (**C**) SHIP-1 knockdown with siRNA shown by flow cytometry (relative median fluorescence intensity and histogram) and Western blot analysis (**D**) in mBMMCs electroporated with SHIP-1-specific siRNA, control siRNA (NC), blank control (B), and nonelectroporated (NE). (**E**) β-Hexosaminidase release for DNP-HSA activated (Act), desensitized (Desens), or challenged HSA siRNA SHIP-1 BMMCs in each condition. (**F**) Percentage of β-hexosaminidase release inhibited by desensitization, calculated by the formula $(\%AC - \%DS)/\%AC$, in each group of siRNA SHIP-1 BMMCs. $*p < 0.05$, $**p < 0.01$, $***p < 0.001$. $n = 3$ independent experiments. (**G**) Cre SHIP-1 fl/fl BMMCs incubated with Tat to flox SHIP-1 protein were activated with DNP-HSA, desensitized with DNP-HSA, and control activated with HSA, and degranulation was calculated with LAMP-1 expression (**H**) Efficiency of desensitization in Cre SHIP-1 fl/fl BMMC activated, desensitized, and control. $n = 3$ experiments. $*p < 0.05$, $**p < 0.01$, $***p < 0.001$. $n = 3$ independent experiments.

desensitized FcεRI would remain unavailable to restore dual phosphorylation of β- and γ-ITAMs and could not engage Syk and other activation partners.

In this model, the complex choreography of desensitization involves a skewing to inhibitory signals initiated by suboptimal Ag, which generate iITAMs and favor the docking of SHIP-1 over Syk through engagement of single SH2 domains. Removing SHIP-1 protein decreased the inhibitory function of desensitization, indicating the need for structurally intact protein because its phosphatase activity was not involved. Multiple suboptimal Ag doses below 10% of the optimal dose would saturate all FcεRI iITAMs sensitized with the specific desensitizing Ag, and a minimal time of 10 min between doses would allow rearrangement of the membrane and segregation of crosslinked FcεRI from activation partners. Membrane segregation of desensitized FcεRI would allow nondesensitized Ags to access the activation machinery (Fig. 2C).

This study provides evidence that SHIP-1 is required for desensitization and that the initiation of inhibitory signals is upstream and

independent of its phosphatase function. Many questions remain unanswered, including which inhibitory partners are activated by SHIP-1 during desensitization, how desensitized and crosslinked are FcεRI segregated, and how segregation is maintained to preclude specific activation signaling. Although this study does not provide evidence of the generation of iITAMs, it provides evidence of SHIP-1 involvement, opening the field for a targeted approach to the inhibitory mechanisms underlying multistep desensitizations. SHIP-1 is shown to participate in the delicate balance between activation and desensitization, and interventions promoting SHIP-1 activation would enhance the inhibitory state and help design safer human protocols. Uncovering SHIP-1 as a player in multistep IgE desensitization provides insight into a "biological brake" of mast cell activation and anaphylaxis with therapeutic potential.

Acknowledgments

The authors acknowledge Kylie Besz for superb technical skills with the manuscript and references. The visual abstract was created with BioRender.com.

Disclosures

The authors have no financial conflicts of interest.

References

1. Ang, W. X., A. M. Church, M. Kulis, H. W. Choi, A. W. Burks, and S. N. Abraham. 2016. Mast cell desensitization inhibits calcium flux and aberrantly remodels actin. *J. Clin. Invest.* 126: 4103–4118.
2. Oka, T., E. J. Rios, M. Tsai, J. Kalesnikoff, and S. J. Galli. 2013. Rapid desensitization induces internalization of antigen-specific IgE on mouse mast cells. *J. Allergy Clin. Immunol.* 132: 922–932.e16.
3. Sancho-Serra, M. C., M. Simarro, and M. Castells. 2011. Rapid IgE desensitization is antigen specific and impairs early and late mast cell responses targeting FcεRI internalization. *Eur. J. Immunol.* 41: 1004–1013.
4. Isabwe, G. A. C., M. Garcia Neuer, L. de Las Vecillas Sanchez, D. M. Lynch, K. Marquis, and M. Castells. 2018. Hypersensitivity reactions to therapeutic monoclonal antibodies: phenotypes and endotypes. *J. Allergy Clin. Immunol.* 142: 159–170.e2
5. Land, M. H., E. H. Kim, and A. W. Burks. 2011. Oral desensitization for food hypersensitivity. *Immunol. Allergy Clin. North Am.* 31: 367–376.
6. Legere III, H. J., R. I. Palis, T. Rodriguez Bouza, A. Z. Uluer, and M. C. Castells. 2009. A safe protocol for rapid desensitization in patients with cystic fibrosis and antibiotic hypersensitivity. *J. Cyst. Fibros.* 8: 418–424.
7. Sloane, D., U. Govindarajulu, J. Harrow-Mortelliti, W. Barry, F. I. Hsu, D. Hong, T. Laidlaw, R. Palis, H. Legere, S. Bunyavanich, et al. 2016. Safety, costs, and efficacy of rapid drug desensitizations to chemotherapy and monoclonal antibodies. *J. Allergy Clin. Immunol. Pract.* 4: 497–504.
8. Herlihy, L., E. H. Kim, A. W. Burks, H. Barber, Q. Cook, L. Yang, D. Hamilton, and B. P. Vickery. 2021. Five-year follow-up of early intervention peanut oral immunotherapy. *J. Allergy Clin. Immunol. Pract.* 9: 514–517.
9. Vickery, B. P., A. Vereda, T. B. Casale, K. Beyer, G. du Toit, J. O. Hourihane, S. M. Jones, W. G. Shreffler, A. Marcantonio, R. Zawadzki, et al.; PALISADE Group of Clinical Investigators. 2018. AR101 oral immunotherapy for peanut allergy. *N. Engl. J. Med.* 379: 1991–2001.
10. Castells, M. 2017. Drug hypersensitivity and anaphylaxis in cancer and chronic inflammatory diseases: the role of desensitizations. *Front. Immunol.* 8: 1472.
11. Kinet, J. P. 1999. The high-affinity IgE receptor (Fc epsilon RI): from physiology to pathology. *Annu. Rev. Immunol.* 17: 931–972.
12. Rivera, J., and A. M. Gilfillan. 2006. Molecular regulation of mast cell activation. *J. Allergy Clin. Immunol.* 117: 1214–1225, quiz 1226.
13. Andrews, N. L., J. R. Pfeiffer, A. M. Martinez, D. M. Haaland, R. W. Davis, T. Kawakami, J. M. Oliver, B. S. Wilson, and D. S. Lidke. 2009. Small, mobile FcepsilonRI receptor aggregates are signaling competent. *Immunity* 31: 469–479.
14. Draber, P., I. Halova, I. Polakovicova, and T. Kawakami. 2016. Signal transduction and chemotaxis in mast cells. *Eur. J. Pharmacol.* 778: 11–23.
15. Morales, A. R., N. Shah, and M. Castells. 2005. Antigen-IgE desensitization in signal transducer and activator of transcription 6-deficient mast cells by suboptimal doses of antigen. *Ann. Allergy Asthma Immunol.* 94: 575–580.
16. MacGlashan, D., Jr., and N. Vilariño. 2006. Nonspecific desensitization, functional memory, and the characteristics of SHIP phosphorylation following IgE-mediated stimulation of human basophils. *J. Immunol.* 177: 1040–1051.
17. Harmon, B., L. A. Chylek, Y. Liu, E. D. Mitra, A. Mahajan, E. A. Saada, B. R. Schudel, D. A. Holowka, B. A. Baird, B. S. Wilson, et al. 2017. Timescale separation of positive and negative signaling creates history-dependent responses to IgE receptor stimulation. *Sci. Rep.* 7: 15586.
18. Huber, M., C. D. Helgason, M. P. Scheid, V. Duronio, R. K. Humphries, and G. Krystal. 1998. Targeted disruption of SHIP leads to Steel factor-induced degranulation of mast cells. *EMBO J.* 17: 7311–7319.
19. Nakata, K., T. Yoshimaru, Y. Suzuki, T. Inoue, C. Ra, H. Yakura, and K. Mizuno. 2008. Positive and negative regulation of high affinity IgE receptor signaling by Src homology region 2 domain-containing phosphatase 1. *J. Immunol.* 181: 5414–5424.
20. Torigoe, C., J. R. Faeder, J. M. Oliver, and B. Goldstein. 2007. Kinetic proofreading of ligand-FcepsilonRI interactions may persist beyond LAT phosphorylation. *J. Immunol.* 178: 3530–3535.
21. Wilson, B. S., J. R. Pfeiffer, Z. Surviladze, E. A. Gaudet, and J. M. Oliver. 2001. High resolution mapping of mast cell membranes reveals primary and secondary domains of Fc(epsilon)RI and LAT. *J. Cell Biol.* 154: 645–658.
22. Castells, M. C., L. B. Klickstein, K. Hassani, J. A. Cumplido, M. E. Lacouture, K. F. Austen, and H. R. Katz. 2001. gp49B1-alpha(v)beta3 interaction inhibits antigen-induced mast cell activation. *Nat. Immunol.* 2: 436–442.
23. Daëron, M., S. Jaeger, L. Du Pasquier, and E. Vivier. 2008. Immunoreceptor tyrosine-based inhibition motifs: a quest in the past and future. *Immunol. Rev.* 224: 11–43.
24. Fung-Leung, W. P., J. De Sousa-Hitzler, A. Ishaque, L. Zhou, J. Pang, K. Ngo, J. A. Panakos, E. Chourmouzis, F. T. Liu, and C. Y. Lau. 1996. Transgenic mice expressing the human high-affinity immunoglobulin (Ig) E receptor alpha chain respond to human IgE in mast cell degranulation and in allergic reactions. *J. Exp. Med.* 183: 49–56.
25. Moñino-Romero, S., L. L. Vecillas, L. A. Alenazy, M. Labella, Z. Szépfalusi, E. Fiebiger, and M. C. Castells. 2020. Soluble FcεRI, IgE, and tryptase as potential biomarkers of rapid desensitizations for platin IgE sensitized cancer patients. *J. Allergy Clin. Immunol. Pract.* 8: 2085–2088.e10.
26. Dombrowicz, D., A. T. Brini, V. Flamand, E. Hicks, J. N. Snouwaert, J. P. Kinet, and B. H. Koller. 1996. Anaphylaxis mediated through a humanized high affinity IgE receptor. *J. Immunol.* 157: 1645–1651.
27. Yokota, T., F. Lee, D. Rennick, C. Hall, N. Arai, T. Mosmann, G. Nabel, H. Cantor, and K. Arai. 1984. Isolation and characterization of a mouse cDNA clone that expresses mast-cell growth-factor activity in monkey cells. *Proc. Natl. Acad. Sci. USA* 81: 1070–1074.
28. Kirshenbaum, A.S., C. Akin, Y. Wu, M. Rottem, J. P. Goff, M. A. Beaven, V. K. Rao, and D. D. Metcalfe. 2003. Characterization of novel stem cell factor responsive human mast cell lines LAD 1 and 2 established from a patient with mast cell sarcoma/leukemia; activation following aggregation of FcεRI or FcγRI. [Published erratum appears in 2003 *Leuk. Res.* 27: 1171] *Leuk. Res.* 27: 677–682.
29. Nishida, K., S. Yamasaki, Y. Ito, K. Kabu, K. Hattori, T. Tezuka, H. Nishizumi, D. Kitamura, R. Goitsuka, R. S. Geha, et al. 2005. FcεRI-mediated mast cell degranulation requires calcium-independent microtubule-dependent translocation of granules to the plasma membrane. *J. Cell Biol.* 170: 115–126.
30. Grützkau, A., A. Smorodchenko, U. Lippert, L. Kirchhof, M. Artuc, and B. M. Henz. 2004. LAMP-1 and LAMP-2, but not LAMP-3, are reliable markers for activation-induced secretion of human mast cells. *Cytometry A* 61: 62–68.
31. Hundley, T. R., A. M. Gilfillan, C. Tkaczyk, M. V. Andrade, D. D. Metcalfe, and M. A. Beaven. 2004. Kit and FcepsilonRI mediate unique and convergent signals for release of inflammatory mediators from human mast cells. *Blood* 104: 2410–2417.
32. Oka, T., M. Hori, A. Tanaka, H. Matsuda, H. Karaki, and H. Ozaki. 2004. IgE alone-induced actin assembly modifies calcium signaling and degranulation in RBL-2H3 mast cells. *Am. J. Physiol. Cell Physiol.* 286: C256–C263.
33. Deng, Z., T. Zink, H. Y. Chen, D. Walters, F. T. Liu, and G. Y. Liu. 2009. Impact of actin rearrangement and degranulation on the membrane structure of primary mast cells: a combined atomic force and laser scanning confocal microscopy investigation. *Biophys. J.* 96: 1629–1639.
34. Hájková, Z., V. Bugajev, E. Dráberová, S. Vinopal, L. Dráberová, J. Janáček, P. Dráber, and P. Dráber. 2011. STIM1-directed reorganization of microtubules in activated mast cells. *J. Immunol.* 186: 913–923.
35. Siraganian, R. P., R. O. de Castro, E. A. Barbu, and J. Zhang. 2010. Mast cell signaling: the role of protein tyrosine kinase Syk, its activation and screening methods for new pathway participants. *FEBS Lett.* 584: 4933–4940.
36. Mahajan, A., D. Barua, P. Cutler, D. S. Lidke, F. A. Espinoza, C. Pehlke, R. Grattan, Y. Kawakami, C. S. Tung, A. R. Bradbury, et al. 2014. Optimal aggregation of FcεRI with a structurally defined trivalent ligand overrides negative regulation driven by phosphatases. *ACS Chem. Biol.* 9: 1508–1519.
37. Rohrschneider, L. R., J. F. Fuller, I. Wolf, Y. Liu, and D. M. Lucas. 2000. Structure, function, and biology of SHIP proteins. *Genes Dev.* 14: 505–520.
38. Castells, M. 2009. Rapid desensitization for hypersensitivity reactions to medications. *Immunol. Allergy Clin. North Am.* 29: 585–606.
39. Pauls, S. D., and A. J. Marshall. 2017. Regulation of immune cell signaling by SHIP1: a phosphatase, scaffold protein, and potential therapeutic target. *Eur. J. Immunol.* 47: 932–945.
40. Osborne, M. A., G. Zenner, M. Lubinus, X. Zhang, Z. Songyang, L. C. Cantley, P. Majerus, P. Burn, and J. P. Kochan. 1996. The inositol 5′-phosphatase SHIP binds to immunoreceptor signaling motifs and responds to high affinity IgE receptor aggregation. *J. Biol. Chem.* 271: 29271–29278.
41. Getahun, A., and J. C. Cambier. 2015. Of ITIMs, ITAMs, and ITAMis: revisiting immunoglobulin Fc receptor signaling. *Immunol. Rev.* 268: 66–73.